

Observer-based disturbance suppression in a 3-DoF positioning system for high-precision 3D inline metrology

Daniel Pechgraber^{*†}, Ernst Csencsics^{*†} and Georg Schitter^{*}

^{*}Automation and Control Institute (ACIN)

TU Wien, Vienna, Austria

Email: pechgraber@acin.tuwien.ac.at

[†] Christian Doppler Laboratory for Precision Measurements in Motion, Automation and Control Institute

TU Wien, Vienna, Austria

Abstract—This paper proposes an advanced disturbance-suppression strategy for a dual-stage actuated 3-degree-of-freedom (3-DoF) positioning system for high-precise optical 3D inline metrology applications. The decentralized control loop based on single input single output (SISO) PID controllers is complemented by a disturbance observer (DOB) in each DoF to suppress disturbance forces, originating from the coarse positioning unit at fractions of the pitch of the mechanical spindle drive. By reformulating the DOB design problem in the H_∞ -synthesis framework, the disturbance sensitivity of the closed-loop system is shaped to suppress disturbances at these specific frequencies. Experiments on an experimental prototype demonstrate the effectiveness of the approach with up to 28% reduction of measurement errors related to the positioning system on a large inspection area (0.7x0.6m).

I. INTRODUCTION

Inline measurement systems are an indispensable component of modern industrial manufacturing and production processes, given the increasing demand for precision, throughput and continuous quality control [1]. Consequently, optical 3D measurement systems, such as laser line or structured light sensors, are frequently employed in a multitude of applications with moderate precision requirements [2], [3]. Nevertheless, they are facing more and more challenges in terms of increasing speed and precision demands in advanced production systems, as the measurement precision is significantly limited by motion blur [4].

One solution to this problem is to precisely position the optical measurement system with respect to the measurement sample in order to enable high-precision 3D surface measurements on moving objects [5]. This results in local lab-like conditions, wherein the relative motion between sample and measurement system is ideally zero. Furthermore, the measurement range can be arbitrarily extended within the capabilities of the positioning system, which is beneficial when moving laser-line sensors over measurement samples to obtain 3D surface measurements [6]. Nevertheless, the measurement precision in the moving direction depends heavily on the positioning system, especially considering parasitic rotational

motions of the measurement system with respect to the motion plane of the sample.

For precise positioning over long distances dual-stage actuation is often used, combining a coarse, long-range actuator with a fine, high-precision actuator, as seen in applications ranging from hard disk drives to wafer scanners [7], [8]. Fine actuators such as Lorentz actuators (LAs) are particularly well suited due to their quasi-zero stiffness, which helps to isolate disturbances from coarse-stage motion [9]–[11]. The moving part is usually constrained in the non-actuated DoFs by either magnetic levitation or air-bearings [5], [12] to keep the zero stiffness property, or by mechanical flexure structures in combination with a position control loop [13].

A recently proposed 3-DoF positioning system for optical inline metrology combines a mechanical spindle drive and 3 LAs to precisely move a metrology platform over a production line while also maintaining a constant orientation to the sample motion by position control in 3 DoFs [14]. While disturbance forces from the coarse-actuator are isolated by the LAs, errors related to the mechanical periodicity of the spindle-drive are still transmitted to the metrology platform via the surrounding machine frame.

A widely adopted approach for suppressing external disturbance in motion control loops are disturbance observers (DOB) [15]. While classically an inverted plant model in combination with a tuned low-pass filter (Q -filter) is used for estimating external disturbances, it is shown that the DOB design can also be formulated in the H_∞ -synthesis framework [16]. By applying appropriate weighting filters for the H_∞ -synthesis, this method can be used to suppress disturbances at specific frequencies, as e.g. applied to hard-disk drives in [17].

The contribution of this paper is an advanced disturbance-suppression strategy targeting periodic errors from the coarse stage's mechanical spindle in a dual-stage actuated, 3-DoF positioning system for high-precise inline metrology. Classical PID position control is enhanced with DOBs designed in the H_∞ -framework, with performance improvements demonstrated on an experimental prototype.

The remainder of the paper is organized as follows: Section II and Section III introduce the dual-stage actuated 3-DoF positioning system and a decentralized motion control strategy based on modal decoupling, which is then extended by the proposed DOB-control in Section IV. Section V provides the experimental validation of the approach and Section VI concludes the paper.

II. MULTI-DOF POSITIONING SYSTEM

A. Principle of operation

In Fig. 1 a principle sketch of an optical 3D inline measurement system is shown, which incorporates a movable metrology platform, carrying optical measurement systems. The coarse actuator provides long travel range in y -direction

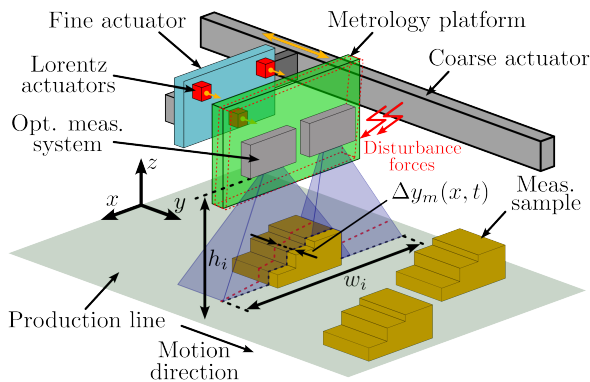


Fig. 1. Principle of optical 3D inline measurement system with moving optical measurement systems. Multiple fine-actuators move the metrology platform in y -direction and control the orientation relative to the production line. Disturbance forces on the metrology platform lead to a lateral measurement error of $\Delta y_m(x, t)$.

to cover a large inspection area, while the LAs on the fine-actuator control the translational motion and rotation of the metrology platform in the relevant DoFs by applying forces at 3 points from the back. External disturbance forces acting on the metrology platform can induce unwanted parasitic motion, which leads to a measurement errors in motion direction $\Delta y_m(x, t)$.

B. System design and prototype

For the subsequent evaluations an experimental prototype of the positioning system is built, as shown in Fig. 2 [14]. Core part of the system is the metrology platform carrying the measurement systems (not mounted), which is moved along the y -direction. A spindle-drive with a stepper motor is used for coarse positioning, providing extendable travel ranges and reducing system costs. To overcome the low positioning precision of mechanical spindle-drives, a dual-stage approach is applied. Therefore the coils of 3 cylindrical LAs are mounted on the pusher, which is connected to the spindle-drive. The magnet parts of the LAs are fixed at the metrology platform, allowing the positioning of the stage in 3DoFs (y, θ, ψ). The LA forces are proportional to their currents, which are

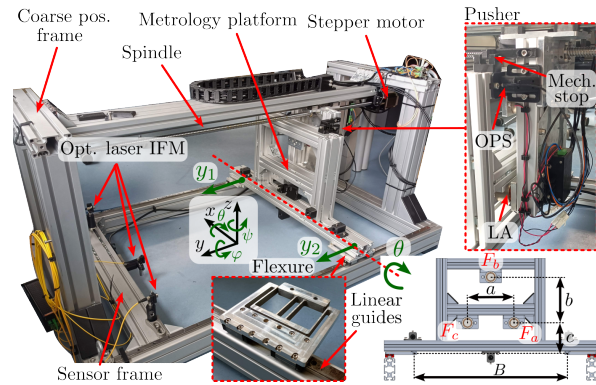


Fig. 2. 3-DoF dual actuated positioning system. The coarse actuator consists of a mechanical spindle-drive with stepper motor, which drives the pusher, on which 3 LAs are mounted for the fine-motion. The metrology platform is guided on mechanical flexure mounts [14].

controlled by high-bandwidth current controllers ($f_b = 5$ kHz) and custom-made switched amplifiers [18].

The stage is suspended on the machine frame by linear roller guides on either side of the frame. To counteract manufacturing and mounting tolerances of the linear guides, the stage is guided on mechanical flexure mounts, which enable sufficient motion freedom in the actuated DoFs, while providing sufficient stiffness in the non-actuated DoFs [14]. Additionally, mechanical stops are added, which restrict the relative motion between the pusher and the metrology platform, to keep the flexures within their mechanical stress limits.

Position measurement of the stage is done via 3 optical laser interferometers (IFM) (IDS3010, AttoCube Systems AG, GER) mounted on the sensor frame and the difference position between stage and pusher is measured by an optical proximity sensor (OPS) (TCND5000, Vishay, US). The sensor readout and subsequent derived control algorithms are implemented on a rapid prototyping system (MicroLab-Box, dSPACE GmbH, GER) with a sample-rate of 50 kHz.

III. DECOUPLED DUAL-STAGE CONTROL

A. System model

A full (non-linear) system model of the metrology platform movement is derived in [14]. It is shown, that during stage motion, a simplified linear model with the coordinates $\mathbf{q} = [y_1 \ y_2 \ \theta]^T$ (refer to Fig. 2) approximates the real behavior sufficiently well for the subsequent control design. The model can be formulated as a coupled linear mechanical system

$$\mathbf{M}\ddot{\mathbf{q}} + \mathbf{D}\dot{\mathbf{q}} + \mathbf{K}\mathbf{q} = \mathbf{W}\mathbf{f}^e, \quad (1)$$

with the constant mass matrix $\mathbf{M} \in \mathbb{R}^{3 \times 3}$, damping matrix $\mathbf{D} \in \mathbb{R}^{3 \times 3}$, stiffness matrix $\mathbf{K} \in \mathbb{R}^{3 \times 3}$, and the LA force vector $\mathbf{f}^e = [F_a \ F_b \ F_c]^T$ which is mapped to the generalized forces with the constant matrix

$$\mathbf{W} = \begin{bmatrix} \frac{a+B}{2B} & \frac{1}{2} & \frac{-a+B}{2B} \\ -\frac{a+B}{2B} & \frac{1}{2} & \frac{a+B}{2B} \\ -c & -c-b & -c \end{bmatrix}. \quad (2)$$

The system matrices in dependence of the system parameters are given by [14]

$$\begin{aligned}
 \mathbf{m}_1 &= \begin{bmatrix} \frac{m_p(B^2+4Bx_g+4x_g^2+4y_g^2)+4I_{zz}}{4B^2} \\ \frac{m_p(B^2-4x_g^2-4y_g^2)-4I_{zz}}{4B^2} \\ -\frac{m_p z_g(B+2x_g)}{2B} \end{bmatrix}, \\
 \mathbf{m}_2 &= \begin{bmatrix} \frac{m_p(B^2-4x_g^2-4y_g^2)-4I_{zz}}{4B^2} \\ \frac{m_p(B^2+4Bx_g+4x_g^2+4y_g^2)+4I_{zz}}{4B^2} \\ -\frac{m_p z_g(B-2x_g)}{2B} \end{bmatrix}, \\
 \mathbf{m}_3 &= \begin{bmatrix} -\frac{m_p z_g(B+2x_g)}{2B} \\ -\frac{m_p z_g(B-2x_g)}{2B} \\ m_p(y_g^2+z_g^2)+I_{xx} \end{bmatrix}, \\
 \mathbf{K} &= \begin{bmatrix} \frac{2k_2}{B^2} & -\frac{2k_2}{B^2} & \frac{m_p x_g g}{B} \\ -\frac{2k_2}{B^2} & \frac{2k_2}{B^2} & -\frac{m_p x_g g}{B} \\ \frac{m_p x_g g}{B} & -\frac{m_p x_g g}{B} & -gm_p z_g + 2k_3 \end{bmatrix}, \\
 \mathbf{D} &= \begin{bmatrix} r_v + \frac{4d_2}{B^2} & -\frac{4d_2}{B^2} & 0 \\ -\frac{4d_2}{B^2} & r_v + \frac{4d_2}{B^2} & 0 \\ 0 & 0 & d_3 \end{bmatrix}.
 \end{aligned} \tag{3}$$

B. System decoupling

In order to apply a decentralized position control scheme with separate SISO controllers for each DoF, the linear coupled mechanical system (1) is decoupled by a modal analysis approach [19]. This means, that a decoupling matrix \mathbf{U} is obtained, which transforms the coordinates \mathbf{q} in modal coordinates $\nu = \mathbf{U}^{-1}\mathbf{q}$, for which ideally the equations of motion are decoupled. For undamped system the solution of the generalized eigenvalue problem

$$\lambda^2 \mathbf{M}\mathbf{u} = \mathbf{K}\mathbf{u}, \quad \mathbf{U} = [\mathbf{u}_1 \quad \mathbf{u}_2 \quad \dots \quad \mathbf{u}_n] \tag{4}$$

directly leads to \mathbf{U} , which decouples the \mathbf{M} and \mathbf{K} matrix from (1) [19]. Although the damping matrix \mathbf{D} of (1) is not decoupled by \mathbf{U} in this case, this approach can still be used, since the controller can deal with the remaining coupling via the damping matrix [14]. After solving (4) and normalizing \mathbf{U} , such that $\mathbf{U}^T \mathbf{M} \mathbf{U} = \mathbf{I}$, the equations of motion in the modal coordinates ν can be written as

$$\underbrace{\mathbf{U}^T \mathbf{M} \mathbf{U}}_{\mathbf{M}_{dec}=\mathbf{I}} \ddot{\nu} + \underbrace{\mathbf{U}^T \mathbf{D} \mathbf{U}}_{\mathbf{D}'} \dot{\nu} + \underbrace{\mathbf{U}^T \mathbf{K} \mathbf{U}}_{\mathbf{K}_{dec}} \nu = \underbrace{\mathbf{U}^T \mathbf{W} \mathbf{f}^e}_{\mathbf{f}_{dec}}, \tag{5}$$

with the diagonalized mass- and stiffness matrix (\mathbf{M}_{dec} , \mathbf{K}_{dec}) and the damping matrix \mathbf{D}' , which contains non-zero off-diagonal entries.

C. Dual-stage control

Given the derived system equations (5), 3 separate SISO PID-controllers are designed, to control the metrology platform's position by adjusting the forces in the LAs at the back of the stage. A block-diagram of the implemented control scheme is shown in Fig. 3 [14]. The plant model with the LA forces as input is given with the transfer matrix \mathbf{G} , which is decoupled using the modal matrix \mathbf{U} and the force mapping matrix \mathbf{W} . The grey-box in Fig. 3 represents the decoupled

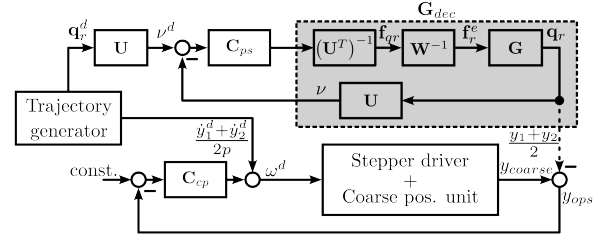


Fig. 3. Dual-stage control concept.

plant \mathbf{G}_{dec} which corresponds to equation (5). Generally, the position controller C_{ps} aims to track the reference position ν^d , which is calculated from the desired motion trajectory for the stage from the trajectory generator \mathbf{q}^d via $\nu^d = \mathbf{U}\mathbf{q}^d$.

To keep the LAs within their actuation range, the coarse positioning controller $C_{cp} = P_{cp}$ (P-control) controls the spindle-drives velocity ω^d by using the difference position signal from the OPS sensor (refer to Fig. 2). Since the desired stage motion is known from the trajectory generation, additionally the desired velocity in y-direction is applied to the spindle-drive in a feed-forward manner together with the mechanical spindle pitch p .

For each modal coordinate ν_j , $j \in \{1, 2, 3\}$ a PID-controller

$$C_{pid}(s) = k_p + \frac{k_{I,p}}{s} + \frac{k_d s}{1 + sT_t}, \tag{6}$$

is designed for an open-loop cross-over frequency of $f_c = 80$ Hz. This frequency is limited by structural modes of the system, starting from approximately 150 Hz [14]. To suppress these non-modeled structural modes at higher frequencies, notch filters

$$C_{n,i}(s) = \frac{s^2 + 2D_i \xi_i \omega_{n,i} s + \omega_{n,i}^2}{s^2 + 2\xi_i \omega_{n,i} s + \omega_{n,i}^2}, \tag{7}$$

are tailored for the respective mode frequencies and the resulting controller is given by

$$C_{ps,jj}(s) = C_{pid}(s) \cdot \prod_i C_{n,i}(s), \quad j \in \{1, 2, 3\}. \tag{8}$$

A summary of the system and tuned controller parameter is given in Table I.

IV. DOB EXTENSION

The zero-stiffness property of the LAs prevents the direct transmission of disturbance forces originating from the coarse positioning unit to the metrology platform. However, since the coarse positioning frame is connected to the machine frame, disturbances are still transmitted to the stage. A characteristic of the disturbance forces from the spindle-drive is their spatial periodicity at fractions of the mechanical spindle pitch [14]. This means, that by knowing the travelling speed of the spindle-drive v , a portion of the generated disturbances can

TABLE I
SYSTEM AND CONTROL PARAMETERS

System parameters			
a	172 mm	b	167 mm
d	12 mm	B	562 mm
p	10 mm	x_g	-3.8 mm
z_g	148 mm	m_p	7.9 kg
k_1	47 200 $\frac{\text{N}}{\text{m}}$	k_2	1700 $\frac{\text{N}}{\text{m}}$
d_1	-4.7 $\frac{\text{N}}{\text{m}}$	d_2	0.28 $\frac{\text{N}}{\text{m}}$
J_{xx}	0.13 kg m ²	J_{yy}	0.41 kg m ²
c	119 mm	k_a	12.7 $\frac{\text{N}}{\text{A}}$
		y_g	-3.4 mm
		m_c	0.22 kg
		k_3	92 $\frac{\text{N}}{\text{m}}$
		d_3	1.12 $\frac{\text{N}}{\text{m}}$
		J_{zz}	0.215 kg m ²
Position controller C_{pid}, P_{cp}			
k_p	$5.6 \cdot 10^4$	k_I	$1.76 \cdot 10^6$
T_t	$4.97 \cdot 10^{-4}$	P_{cp}	$1.35 \cdot 10^3$
		k_d	$4.45 \cdot 10^2$
Notch filter $C_{n,i}(s)$			
$\frac{\omega_{n,i}}{2\pi}$	245, 325, 454, 550, 600, 681, 713, 750		
	796, 930, 1089, 1245, 1815, 2375		
D_i	0.006, 0.01, 0.1, 0.056, 0.018, 0.032, 0.032, 0.316		
	0.1, 0.1, 0.018, 0.032, 0.178, 0.003		
ξ_i	0.25, 0.13, 0.05, 0.15, 0.2, 0.1, 0.1, 0.08		
	0.08, 0.25, 0.15, 0.15, 0.1, 0.8		

be associated to specific frequencies, related to fractions of the mechanical spindle-pitch p according to

$$f_{d,n} = \frac{v}{np}, \quad n \in \{2, 4, 6, \dots\}. \quad (9)$$

Since these frequencies are known, the upper control loop from Fig. 3 is extended by a DOB to suppress these disturbances, as shown in Fig. 4a.

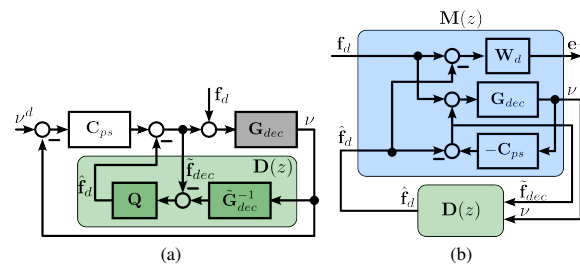


Fig. 4. Extended control scheme. a) Control loop extended with disturbance observer (DOB) consisting of a plant inverse \hat{G}_{dec}^{-1} and a filter Q . b) Augmented system model $M(z)$ with included weight W_d for the DOB design in the H_∞ -synthesis framework.

A. DOB Design in H_∞ -synthesis framework

The DOB takes the measured position vector ν and the decoupled force vector \hat{f}_{dec} at the input, and provides an estimation of the input disturbance force \hat{f}_d , which is subtracted from the control output. Ideally, if $\hat{f}_d = f_d$, the disturbance force f_d is canceled out by the DOB.

Classically the DOB design is done by finding a (causal) approximation of the plant inverse \hat{G}_{dec}^{-1} and a low-pass filter Q , to achieve the required stability and robustness properties [15]. However, it is shown, that the problem of tuning \hat{G}_{dec}^{-1} and Q separately can be reformulated to enable an intuitive tuning based on specific noise suppression requirements [17]. This is done by introducing a new variable $D(z)$ and redrawing the

control loop, as depicted in Fig. 4b. If both formulations are compared, $D(z)$ is constrained in a way

$$D(z) = \begin{bmatrix} D_1(z) \\ -D_1(z)G_{dec}^{-1} \end{bmatrix}, \quad (10)$$

resulting from the conventional structure of DOB. This constraint can however be relaxed, and $D(z)$ directly tuned based on H_∞ -optimization, which allows more flexibility with a larger feasibility region, and therefore smaller γ values in the synthesis [17].

For the H_∞ -synthesis the external disturbance force f_d is defined as disturbance input and the estimation error $e_1 = f_d - \hat{f}_d$ as error output. So if the transfer function from disturbance input to error output $T_f(z) = \frac{e_1}{f_d}$ is small in a certain frequency range, the difference between the estimation and the actual disturbance force is small, leading to a good disturbance suppression. To suppress the disturbance at specific frequencies, a weighting function W_d with the structure

$$W_d = 0.1 \cdot \prod_i \frac{s^2 + 2D\xi_i\omega_i s + \omega_i^2}{s^2 + 2\xi_i\omega_i s + \omega_i^2}, \quad (11)$$

$$D = 10, \xi = 0.01, \omega_i = 2\pi \frac{v}{np}, i \in \{2, 4, \dots, 10\}$$

is introduced, which places notches on each of the first 5 harmonics of the spindle-related external disturbance forces (9), as can be seen in the bottom plot of Fig. 5. For the augmented plant $M(z)$ from Fig. 4b, now a DOB $D(z)$ is designed for each modal coordinate $\nu = [\nu_1, \nu_2, \nu_3]^T$ with the Matlab-command *hinfsyn* [20], which minimizes the H_∞ -norm of $T_f(z)$ according to

$$\arg \min_{D(z) \in \text{causal, stable}} \gamma \quad \text{s.t. } \|T_f(z)\|_\infty < \gamma. \quad (12)$$

It is to note, that while the synthesis of $D(z)$ results in a causal and stable solution for the given system, this may not necessarily be the case for arbitrary systems.

B. Disturbance sensitivity

To analyze the influence of the designed DOB in the closed-loop system, the input disturbance sensitivity functions $|\nu/f_d|$ and complementary sensitivity functions $|\nu/v^d|$ from the closed-loop system are shown in the top 3 plots of Fig. 5. As expected, the disturbance sensitivity function is improved at the frequencies for which the DOB is designed. Additionally, it is notable that the inclusion of the DOB only has a negligible impact on the complementary sensitivity function (reference position tracking), which is a further advantage of the proposed approach. In addition to the theoretical transfer functions (solid curves), a closed-loop system identification is performed by moving the stage along the y-direction and applying frequency sweeps at the reference input and the input disturbance input respectively (dashed curves) [21]. The measurements are in good agreement with the theoretical transfer functions, validating the proposed approach.

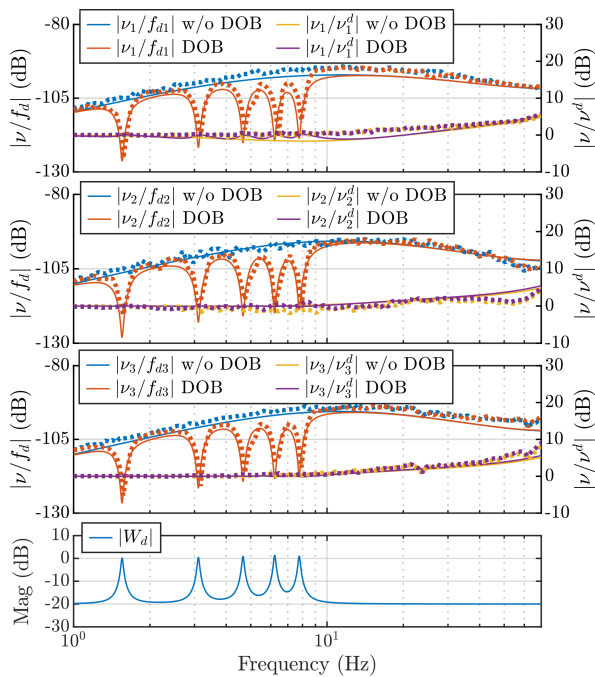


Fig. 5. Input disturbance sensitivity and complementary sensitivity function with and without DOB for a velocity of $8 \frac{\text{mm}}{\text{s}}$. The bottom plot shows the weighting function W_d for the H_∞ -synthesis. The theoretical curves (—), and the measurements from closed-loop MIMO system identification are plotted (----).

V. EXPERIMENTS

A. Measurement errors related to positioning system

For the evaluation of the system, the lateral measurement uncertainty originating from the positioning system is of interest. Therefore, the measured position of the metrology platform is used to calculate the resulting error $\Delta y_m(x, t)$, as shown in Fig. 1. By using $\psi = \tan^{-1} \left(\frac{y_1 - y_2}{B} \right)$, $y_m(x, t)$ can be expressed by

$$\Delta y_m(x, t) = \left[\frac{y_1 + y_2}{2} + h_i \tan(\theta) + x \tan(\psi) \right] - y^d, \quad (13)$$

with the coordinates y_1, y_2, θ and the effective standoff height of the measurement systems h_i . The maximum error along the x-axis is calculated for a given inspection width w_i according to

$$\epsilon_m(t) = \max_x (\Delta y_m(x, t)), \text{ for } x \in \left[-\frac{w_i}{2}, \frac{w_i}{2} \right]. \quad (14)$$

This represents the worst-case measurement error in y-direction over time at any point on the inspection surface. For the subsequent validation $w_i = 0.6 \text{ m}$ and $h_i = 0.55 \text{ m}$ are used, which corresponds to the working distance and field of view of two commercially available 3D surface measurement sensors (SC 2500-300, Micro-Epsilon GmbH, GER) mounted side by side (Fig. 1) [22].

B. Experimental Validation

For the evaluation the metrology platform is moved along the y-direction (Fig. 2) with two different velocities $v \in \{8 \text{ mm/s}, 17 \text{ mm/s}\}$ over a linear travel range of 0.7 m. The measured coordinates (y_1, y_2, θ) are recorded and the worst-case error over the entire inspection are $\epsilon_m(t)$ is calculated according to (14). The power spectral density and the cumulated amplitude spectrum of each measurement is shown in Fig. 6. The plots show, that for each driving velocity the

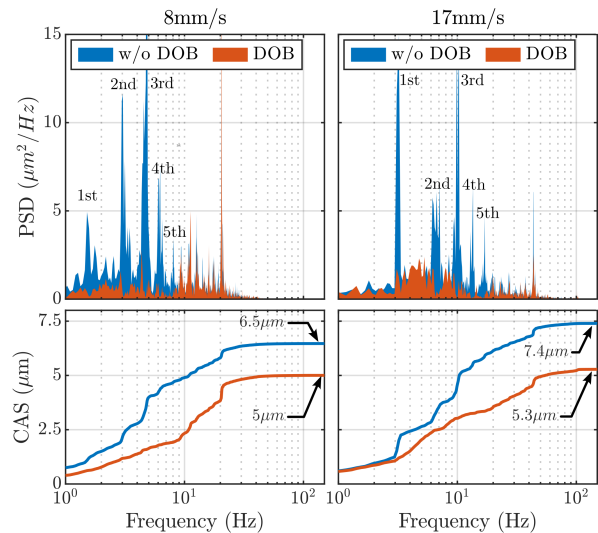


Fig. 6. Power spectral density (PSD) of worst-case measurement error $\epsilon_m(t)$ over frequency and cumulative amplitude spectrum (CAS) for driving speeds of 8 mm/s and 17 mm/s.

first 5 harmonics of the error are vastly reduced with the inclusion of the DOB (red) as compared to the measurements without DOB (blue). The reason for the different PSD levels in the range 10 Hz-20 Hz in the left plot may be due to the fact, that external disturbances are varying between different measurement runs.

In summary, with the inclusion of the DOB in the control loop, the worst-case measurement error coming from the positioning system can be reduced by up to 28 %, demonstrating the effectiveness of the proposed approach to suppress external disturbance forces originating from the mechanical spindle-drive. The measured errors are summarized in Table II.

TABLE II
MAXIMUM MEASUREMENT ERRORS ϵ_m (RMS)

	w/o DOB	DOB	Improvement
8 mm/s	6.5 μm	5 μm	23 %
17 mm/s	7.4 μm	5.3 μm	28 %

VI. CONCLUSION

In this paper an advanced disturbance suppression strategy is proposed for a dual-stage actuated 3-DoF positioning system

for high-precision 3D inline metrology. The motion of the metrology platform is controlled by 3 decoupled SISO control loops consisting of tailored PID controllers and notch filters to suppress structural modes of the system. To suppress errors at fractions of the pitch of the mechanical spindle-drive, each control loop is complemented by a DOB. By reformulating the DOB design in the H_∞ synthesis framework, the disturbance sensitivity of the closed-loop system is shaped in such a way, that disturbances at these specific frequencies are suppressed. Experiments on the experimental prototype are carried out on a large inspection area (0.7x0.6m), which validate the effectiveness of the proposed approach. A 28% reduction of measurement errors related to the positioning system down to 5 μm (rms) is demonstrated for the investigated driving speeds.

ACKNOWLEDGMENTS

The financial support by the Austrian Federal Ministry of Labour and Economy, the National Foundation for Research, Technology and Development and the Christian Doppler Research Association, and Micro-Epsilon Atensor GmbH and MICRO-EPSILON-MESSTECHNIK GmbH & Co.K.G. is gratefully acknowledged.

REFERENCES

- [1] D. Imkamp, R. Schmitt, and J. Berthold, "Blick in die Zukunft der Fertigungsmesstechnik," *Technisches Messen*, vol. 79, no. 10, pp. 433–439, 2012.
- [2] L. Traxler, L. Ginner, S. Breuss, and B. Blaschitz, "Experimental comparison of optical inline 3d measurement and inspection systems," *IEEE Access*, vol. 9, pp. 53 952–53 963, 2021.
- [3] M. Marxer, C. Bach, and C. P. Keferstein, *Fertigungsmesstechnik*. Springer, 2021.
- [4] P. Zanuttigh, G. Marin, C. D. Mutto, F. Dominio, L. Minto, and G. M. Cortelazzo, *Time-of-Flight and Structured Light Depth Cameras : Technology and Applications*. Springer, 2016, p. 367.
- [5] D. Wertjanz, E. Csencsics, T. Kern, and G. Schitter, "Bringing the lab to the fab: Robot-based inline measurement system for precise 3-d surface inspection in vibrational environments," *IEEE Trans. Ind. Electron.*, vol. 69, no. 10, pp. 10 666–10 673, 2022.
- [6] J. Schlarp, E. Csencsics, and G. Schitter, "Optical scanning of laser line sensors for 3d imaging," *Applied Optics*, vol. 57, no. 18, p. 5242, 2018.
- [7] R. Horowitz, Y. Li, K. Oldham, S. Kon, and X. Huang, "Dual-stage servo systems and vibration compensation in computer hard disk drives," *Control Engineering Practice*, vol. 15, no. 3, pp. 291–305, 2007.
- [8] H. Butler, "Position control in lithographic equipment [applications of control]," *IEEE Control Systems*, vol. 31, no. 5, pp. 28–47, 2011.
- [9] N. H. Vrijnsen, J. W. Jansen, and E. A. Lomonova, "Comparison of linear voice coil and reluctance actuators for high-precision applications," in *Proceedings of 14th EPE-PEMC 2010*, IEEE, 2010.
- [10] S. Ito, J. Steininger, and G. Schitter, "Low-stiffness dual stage actuator for long range positioning with nanometer resolution," *Mechatronics*, vol. 29, pp. 46–56, 2015.
- [11] R. M. Schmidt, G. Schitter, and A. Rankers, *The design of high performance mechatronics-: high-Tech functionality by multidisciplinary system integration*. IOS Press, 2020.
- [12] H. Shinno, H. Yoshioka, and H. Sawano, "A newly developed long range positioning table system with a sub-nanometer resolution," *CIRP Annals*, vol. 60, no. 1, pp. 403–406, 2011.
- [13] S. Ito, S. Pirker, and G. Schitter, "Integrating PWM amplifier with the design of mechatronic systems for energy-efficient precision motion," *IEEJ Journal of Industry Applications*, vol. 10, no. 2, pp. 134–141, 2021.
- [14] D. Pechgraber, G. Schitter, and E. Csencsics, "Design, modeling and control of multi degree-of-freedom positioning system for high-precise 3d inline metrology," *Precision Engineering*, (Under Review), 2024.
- [15] E. Sariyildiz, R. Oboe, and K. Ohnishi, "Disturbance observer-based robust control and its applications: 35th anniversary overview," *IEEE Transactions on Industrial Electronics*, vol. 67, no. 3, pp. 2042–2053, 2020.
- [16] C.-C. Wang and M. Tomizuka, "Design of robustly stable disturbance observers based on closed loop consideration using h_{∞} optimization and its applications to motion control systems," in *Proceedings of the 2004 American Control Conference*, IEEE, 2004, 3764–3769 vol.4.
- [17] M. Zheng, S. Zhou, and M. Tomizuka, "A design methodology for disturbance observer with application to precision motion control: An h_{∞} based approach," in *2017 American Control Conference (ACC)*, IEEE, 2017.
- [18] D. Pechgraber, E. Csencsics, J. Wiesböck, and G. Schitter, "Switched amplifier-driven nanopositioning: Integrating system modeling and control tuning," *IEEE Trans. Indust. Electron.*, 2024.
- [19] F. Ma and M. Morzfeld, "A general methodology for decoupling damped linear systems," *Procedia Engineering*, vol. 14, pp. 2498–2502, 2011.
- [20] K. Glover and J. C. Doyle, "State-space formulae for all stabilizing controllers that satisfy an H_{∞} -norm bound and relations to relations to risk sensitivity," *Systems & Control Letters*, vol. 11, no. 3, pp. 167–172, 1988.
- [21] E. Evers, R. Voorhoeve, and T. Oomen, "On frequency response function identification for advanced motion control," in *2020 IEEE 16th International Workshop on Advanced Motion Control (AMC)*, IEEE, 2020.
- [22] Micro-Epsilon GmbH & Co. KG. "Datasheet surface-control 2500 series." (2024), [Online]. Available: <https://www.micro-epsilon.de/fileadmin/download/products/dat--surfaceCONTROL-3D-2500--de.pdf>.